Revealing Regional Disparities: How Fractals Uncover Global Warming's Varied Impact

Sarah K. Zhang

Received March 10, 2024
Accepted April 01, 2024
Electronic access April 15, 2024

In recent years, global warming has become a crisis that affects every region and community. Although often perceived as a universal problem, its impacts vary extensively. The 2015 Paris Agreement acknowledged this reality. This study aims to comprehensively explore the topography and chronology of global warming through fractal geometry. By comparing historical temperature data globally, significant variation in warming rates was demonstrated – from 0.002°C/year in Antarctica to 0.033°C/year in the Arctic. In the US, this range extended from 0.002°C/year in the Midwest to 0.016°C/year on the East Coast. Both the global and domestic variations are linked to uneven atmospheric CO_2 distribution. Rescaled range analysis, a fractal geometry-based method, yielded Hurst exponent ranging from 0.69 to 0.82, reinforcing the ongoing trend of global warming. Temporal analysis of global warming indicated a 0.98°C cooling in Europe in the century preceding industrialization, consistent with the Little Ice Age theory, which subsequently transitioned to a 2.6°C warming in the century following industrialization. No evidence was found to support the "global warming hiatus", which some scientists have invoked to contest the reality of global warming. Interestingly, even the 5.6% CO_2 emission drop during the 2019 COVID-19 lockdown failed to decelerate the rise in atmospheric CO_2 levels and the global warming rate. Overall, this study advocates for a transition from a one-size-fits-all approach to a more nuanced, "global fractal" strategy in tackling global warming. It calls for a more decentralized and sustainable decarbonization effort and underscores the importance of addressing climate inequality through fair and inclusive policies.

Keywords: Global Warming, Fractal Geometry, Heterogeneity, Atmospheric CO_2, COVID-19

Introduction

Climate change refers to the long-term shifts in weather patterns, including temperature, rainfall, and extreme weather events [1,2]. Central to climate change is global warming, the constant increase in Earth's average surface temperature. This complex phenomenon is largely attributed to human activities, such as the rise in greenhouse gas emissions from fossil fuels [3]. These gases trap heat in the atmosphere, leading to higher atmospheric temperatures [4].

Although global warming affects the entire planet, the severity of its impact varies across different regions. Understanding these spatial and temporal differences is essential in creating effective and fair climate policies. However, most research has focused on global impacts, with less attention to regional variations [5,6].

The 2015 Paris Agreement acknowledged this significant variation in global warming. This study aims to comprehensively explore the topography and chronology of global warming through fractal geometry. Fractal Geometry, a mathematical field studying patterns that repeat at different scales, is very useful in climate science [7]. It helps analyze the non-linear and irregular nature of climate data. One key method in this field is rescaled range analysis or Hurst Exponent analysis. It is used in various areas, like hydrology and finance, to identify long-term trends in time series data. A Hurst exponent above 0.5 suggests a continuing trend, while one below 0.5 indicates a likely reversal [8,9].

In this study, fractal methods were used to examine global warming, analyzing temperature and CO_2 level trends since the pre-industrial era. This approach allows for a more detailed understanding of global warming and guides the development of more targeted climate change strategies.

Methodology

Data Collection

I gathered archived temperature data, including monthly mean maximum, mean minimum, and average temperatures, from the Global Summary of the Month (GSOM) Version 1 at the National Centers for Environmental Information (NCEI) database. This data helped analyze global warming's spatial distribution, utilizing the database's map tool to compare meteorological stations across various latitudes and longitudes. Most data series were complete, but the Mawson station in Antarctica had some gaps. To address this, data from the same month in the previous

year were used for continuity in my analysis.

For atmospheric CO_2 concentration, I utilized data from the Global Monitoring Laboratory of the National Oceanic and Atmospheric Administration (GML, NOAA). Global CO_2 emission figures were sourced from Our World In Data's GitHub page. To depict atmospheric CO_2 distribution, I utilized satellite images from the Orbiting Carbon Observatory-2 (OCO-2) at NASA Jet Propulsion Laboratory, obtained from the Environmental System Research Institute (ESRI). Lastly, U.S. demographic data was obtained from the United States Census Bureau.

Deseasonalization

Because the monthly average temperature time series showed annual seasonal cycle, they were deseasonalized using a centered moving average method as described below. In any temperature data time series in this study, each datapoint is the monthly average or mean maximum temperature of a certain month (i) and denoted as T_i.

1. First, a moving average (MA) for each T_i was calculated as:

$$\text{MA of } T_i = \frac{1}{12} \sum_{j=-6}^{5} (T_{i+j})$$

2. Next, a centered moving average (CMA) for each T_i is calculated as:

$$\text{CMA of } T_i = \frac{1}{2} [\text{MA of } T_i + \text{MA of } T_{i+1}]$$

3. Then, each T_i was divided by its centered moving average to calculate a ratio R_i.

4. All R_i for the same month in every year of the entire time series were averaged. This step will generate an average ratio for each of the 12 months in a year. This 12-ratio series repeats every 12 months for the entire series.

5. Next, each ratio generated in step 4 will be adjusted by multiplying by 12 and dividing by the sum of these 12 ratios in a year.

6. Lastly, each T_i is divided by the deseasonalization factor calculated in step 5 to generate deseasonalized T_i.

Rescaled Range Analysis

Rescaled Range Analysis (R/S analysis) was used to study the fractal characteristics of the deseasonalized monthly temperature time series. This was done in Microsoft Excel using the following steps:

1. For any time-series, the last 1024 (2^{10}) datapoints (equivalent to 85.33 years) tracing back from the present time were selected and serially divided into 2^n ($n = 2-8$) equal-length subseries. Thus, each subseries contained 2^{10-n} data points.

2. The means of each subseries were calculated and subtracted from each datapoint to get a mean-adjusted subseries.

3. The cumulative deviation for each datapoint in the corresponding subseries was calculated.

4. Next, the range of cumulative deviation for each subseries was calculated by finding the difference between the minimal and the maximum cumulative deviation for each subseries.

5. The standard deviation of each subseries was calculated.

6. Then the subseries cumulative deviation range was rescaled by dividing it with its standard deviation.

7. The rescaled range of cumulative deviation from all subseries with the same subseries length were averaged.

The $\log_2$ transformed average rescaled ranges were plotted against the $\log_2$ transformed subseries length. A linear relationship in this double-log plot is indicative of a fractal pattern in this range. A simple linear regression was used to fit the Log-Log plot and get the p value and the slope which is the Hurst exponent. The Hurst exponent falls in the range of 0 to 1. If $H > 0.5$, it indicates that the time series has long-term positive autocorrelation, meaning that a high value is more likely to occur after a high value. If $H < 0.5$, it indicates the time series has long-term negative autocorrelation (i.e., mean-reverting), meaning a low value is likely to follow a high value, or vice versa. If $H = 0.5$, it means the time series is random walking and has no long-term persistence.

Statistics

To analyze temperature trends, I conducted simple linear regression in Microsoft Excel and GraphPad Prism (version 10), focusing on the slope of deseasonalized monthly temperature time series to determine the average rate of temperature change. Additionally, I computed the first-degree derivative of these series to assess the instantaneous rate of temperature change.

For long-term trend analysis, I calculated the Hurst exponent by analyzing the linear relationship between $\log_2$-transformed rescaled range and subseries length using simple linear regression in a double-log plot, where the slope represents the Hurst exponent.

In all analyses, a p-value less than 0.05 was considered statistically significant.

Results

Rescaled Range Analysis Revealed a Strong Positive Autocorrelation in Temperature Increase

The temperature change in the last 150 years at Central Park Manhattan, the most populated area in the US, was first analyzed. The monthly average temperature exhibited an annual seasonal cycle, with a central line showing a slow upward shift (Figure 1A). When these data were used for R/S analysis, no linear relationship was observed between the rescaled range versus subseries length in the double-log plot (Figure 1B), indicating that these data were not suitable for R/S analysis.

It was hypothesized that the annual seasonal cycle might cause multifractality and render the data unsuitable for R/S analysis. Therefore, I applied deseasonalization adjustment to these data using the central moving average method, which made the trend of upward shift more easily noticeable (Figure 1C). A simple linear regression yielded a slope of 0.001349 ($p < 0.0001$, $r^2 = 0.15$), equivalent to a 0.016 °C/year warming rate. R/S analysis using the deseasonalized data exhibited a linear relationship between rescaled range and subseries length in the double-log plot, consistent with a fractal pattern (Figure 1D). The Hurst exponent, which is the slope of the fitted line, was 0.67 ($p < 0.0001$), indicating a positive autocorrelation and confirming the warming is a positive autocorrelation. These results highlighted the importance of deseasonalization in the fractal analysis of any time series data with seasonality.

The Spatial Heterogeneity of Global Warming and Northward Polarization of Atmospheric CO_2

The distribution of factors influencing climate change, such as atmospheric CO_2 levels, is not uniform globally. A notable example is the higher concentration of CO_2 in the Northern Hemisphere compared to the Southern Hemisphere, as shown in Figures 2A and 2B. This disparity is mainly due to the Northern Hemisphere's greater landmass and higher number of industrialized countries and urban areas, leading to higher CO_2 emissions. Additionally, the Northern Hemisphere has more vegetation, which absorbs more CO_2 during the summer, resulting in more pronounced seasonal CO_2 fluctuations.

To assess how this northward skew of atmospheric CO_2 affects global warming, temperature changes at Nome, Alaska in the Arctic, and the Mawson Station in Antarctica were analyzed and compared. Before removing seasonal effects, both locations displayed typical annual temperature cycles, albeit with a six-month phase difference (Figure 2C). The Arctic region exhibited a higher baseline temperature and greater oscillation range. The median temperature of the Arctic time series indicated a significant upward shift, contrasting to the nearly imperceptible shift in Antarctica.

Post-deseasonalization, linear regression analysis of the Arctic data revealed a slope of 0.0028 ($p < 0.0001$), corresponding to a warming rate of 0.033 °C/year. In contrast, Antarctica's slope was just 0.00016 ($p = 0.77$), equating to a warming rate of 0.002 °C/year (Figure 2D). Rescaled range (R/S) analysis yielded a Hurst exponent of 0.75 for the Arctic and 0.66 for Antarctica, indicating a stronger warming trend in the Arctic (Figure 2E). These results underscore significant spatial heterogeneity in global warming, with the Arctic experiencing a warming rate approximately 16 times faster than Antarctica.

The Heterogeneity of Global Warming in US

How atmospheric CO_2 levels vary locally and affect microclimates were also analyzed. For instance, NASA's satellite imagery revealed higher CO_2 concentrations on the East and West Coasts of the U.S. compared to the Midwest (Figure 3A). This difference is attributable to factors like different population densities and levels of industrialization. To explore how this uneven CO_2 distribution correlates with microclimate changes, I compared century-long temperature records (1930-present) of Wheatland, Wyoming, and Central Park, Manhattan. Before removing seasonal variations, both locations exhibited similar annual temperature cycles (Figure 3B). However, after deseasonalization, Wheatland showed a ∼6x slower annual warming rate (0.0027°C/year, $p = 0.4395$) compared to Central Park's (0.0162°C/year, $p < 0.0001$ Figure 3C,D).

Many factors can influence microclimates, such as topography, altitude, proximity to water bodies, vegetations, urban heat island (UHI) effect. Although downtown Manhattan has a significantly higher population density, the amount of vegetation, building density, and surface albedo within Central Park are more similar to those in Wheatland Wyoming. Therefore, the UHI effect is significantly reduced within Central Park and is less likely to be the sole contributing factor to the 6x faster warming rate. Additionally, while Wheatland Wyoming is landlocked, the Central Park is much closer to large water bodies which could moderate temperature variations. On the other hand, despite sharing similar latitudes, Wheatland has a much lower population density (326/km^2 vs. 28,830/km^2) and much higher elevation (1,448 m vs. 81 m), which could contribute to its much slower warming rate.

The Temporal Variation of Global Warming

Many factors influencing climate change exhibit significant chronological evolution. Notably, the global atmospheric CO_2 levels were relatively low until the 19th century, when they began rising exponentially following the Industrial Revolution (Figure 4A). To understand how global warming has varied over time, I analyzed historical temperature data from Milan, Italy, dating back to 1763. This analysis differentiated the trend

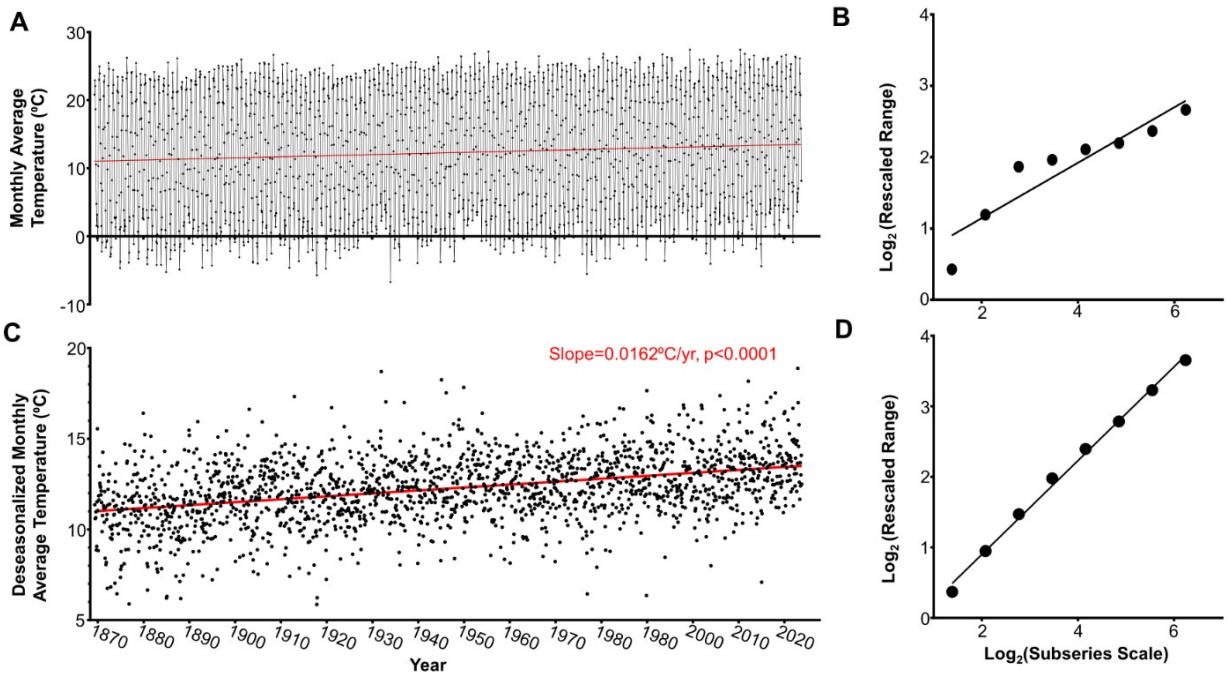

Fig. 1 Analysis of Temperature Trends in Central Park, Manhattan Over 150 Years. **A.** Central Park's monthly average temperature shows an upward-shifting trend within its annual cycle. **B.** Rescaled ranged analysis using non-deseasonalized data reveals no linear relationship. **C.** Post-deseasonalization, linear regression indicates a warming rate of 0.016 °C/year (slope: 0.0013, $p < 0.0001$). **D.** Rescaled range analysis of deseasonalized data displays a linear pattern with a Hurst exponent of 0.67, suggesting the fractal nature and long-term positive autocorrelation in this time series.

of temperature change in pre- and post-Industrial Revolution periods.

Interestingly, the data indicated a period of temperature decrease in Milan before industrialization (Figure 4B). A linear regression showed a cooling rate of -0.010 °C/year ($p<0.0001$) from 1763 to 1862. Rescaled range analysis yielded a Hurst exponent of 0.72 for this period (Figure 4D, blue line), confirming a persistent cooling trend during this time. This finding aligns with the Little Ice Age (LIA) hypothesis, characterized by cooler temperatures in Europe, North America, and parts of Asia from the 1300s to mid-1800s.

However, this cooling trend reversed to a warming trend post-Industrial Revolution. Linear regression identified a warming rate of 0.026 °C/year ($p<0.0001$) from 1863 onwards (Figure 4C), with a Hurst exponent of 0.82, indicating strong and persistent global warming (Figure 4D, red line). Furthermore, the analysis revealed an acceleration in warming since the 21st century, as evidenced by the rising tails in Figure 4C. This contradicts claims of a "Global warming hiatus" and underscores the significant impact of industrialization on the chronological variation of global warming.

Interestingly, the monthly average temperature for each month in a year showed no noticeable change in the pre-industrial era (Figure 4E left, 1763 vs. 1849), but was higher for each month in the post-industrial era (Figure 4E right, 1923 vs. 2006). The temperature increases are more severe from April to September.

The effect of the COVID-19 pandemic on global atmospheric CO_2 level and Global Warming

The impact of COVID-19 pandemic global lockdowns on global warming was specifically examined. In 2019, global CO_2 emissions fell by about 5.6% due to lockdowns [10]. Despite this, there was no noticeable change in the increasing trend of atmospheric CO_2 levels (Figure 4A). This reduction did not affect the rate of change in global warming either, as seen in the first derivative of the deseasonalized monthly average temperature time series. These findings suggest that reducing emissions alone is not sufficient to slow down global warming. A more persistent and intensive approach to decarbonization is necessary. We need to aim for more than just emission cuts to control global warming within the target of 1.5 ºC above pre-industrial levels.

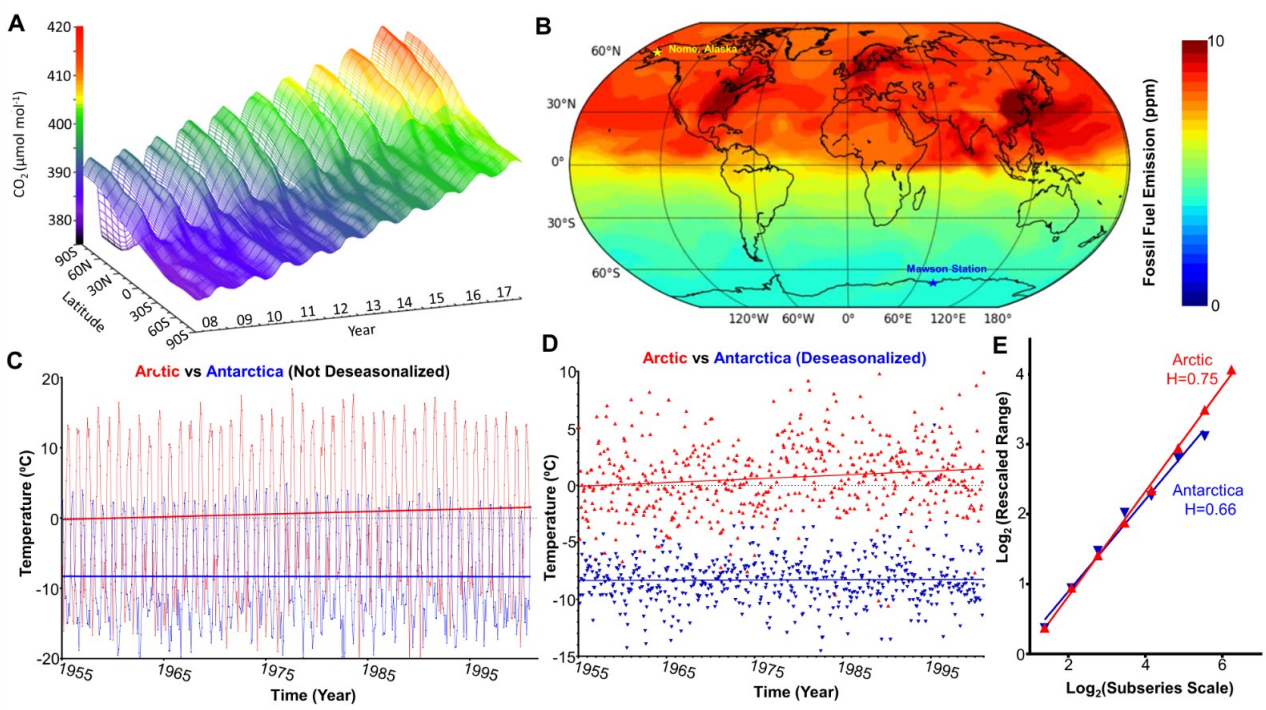

Fig. 2 Global Warming's Spatial Heterogeneity and Atmospheric CO_2 Polarization. **A.** NOAA data showing increasing atmospheric CO_2 levels from 2008-2018, higher and more seasonally variable in the Northern Hemisphere. **B.** Satellite imagery depicts northward polarization of CO_2 from fossil fuels in November 2012. **C.** Comparing Nome, Alaska, and Mawson Station, Antarctica. The Arctic regions show higher baseline temperatures and a more noticeable upward shift. **D.** Deseasonalized data shows the Arctic's higher and faster warming rate (0.033°C/year) compared to Antarctica (0.002°C/year). **E.** Rescaled range analysis indicates a stronger warming trend in the Arctic (Hurst exponent: 0.72) versus Antarctica (0.65).

Discussion

Since Eunice Newton Foote first explained the greenhouse effect in 1856, there has been ongoing debate about global warming. Today, while 97% of scientists agree on it, 20% of the public is still skeptical, leading to political disagreements and inconsistent policies[11]. This study adds fresh insight to this topic using fractal geometry. Originally developed by Harold Edwin Hurst for forecasting the Nile River's dry and draught period[8], Hurst exponent analysis is an invaluable tool in identifying long-term memory within time series data. It can detect both linear and non-linear trends and is robust in non-stationary time series and data with non-normal distribution. Because it is sensitive to sample size, this study analyzed time series longer than a century to ensure robustness. Unlike perfect mathematical fractals, real-world fractal patterns only exist within certain ranges. By using annual average temperature, Bodri et al. showed that global temperatures have a fractal range of 10-10^6 years[12]. This study, using adjusted monthly temperatures, extends this range to as short as four months.

Hurst exponent analysis has some limitations. Firstly, it assumes the trend is intrinsic to the data and overlooks external factors. Many external factors can influence climate, such as solar radiation, volcanic eruptions, the El niño Southern Oscillation (ENSO) etc. Although ENSO is primarily concentrated around the Pacific Equator, it can impact climate globally. During the El niño phase, the warmer surface water in the Pacific Ocean releases more heat into the atmosphere and amplifies global warming. Concurrently, global warming can increase the intensity and modify the frequency of ENSO[13,14]. Although they often act synergistically, global warming and ENSO are driven by different mechanisms and operate on different time scales. Global warming is mostly driven by anthropogenic GHGs emission, thus presenting a more continuous and long-lasting trend. In contrast, ENSO usually occurs every 2-7 years and lasts 9-12 months per cycle, therefore is relatively more episodic. It would be interesting to delineate how the effect of ENSO superimposes on global warming using more sophisticated analysis methods. For example, STL (Seasonal-Trend Decomposition using Locally Estimated Scatterplot Smoothing) can provide more detailed decomposition to detect more transient anomalies such as ENSO. Wavelet analysis can also provide higher resolution of transient signals in both time and frequency do-

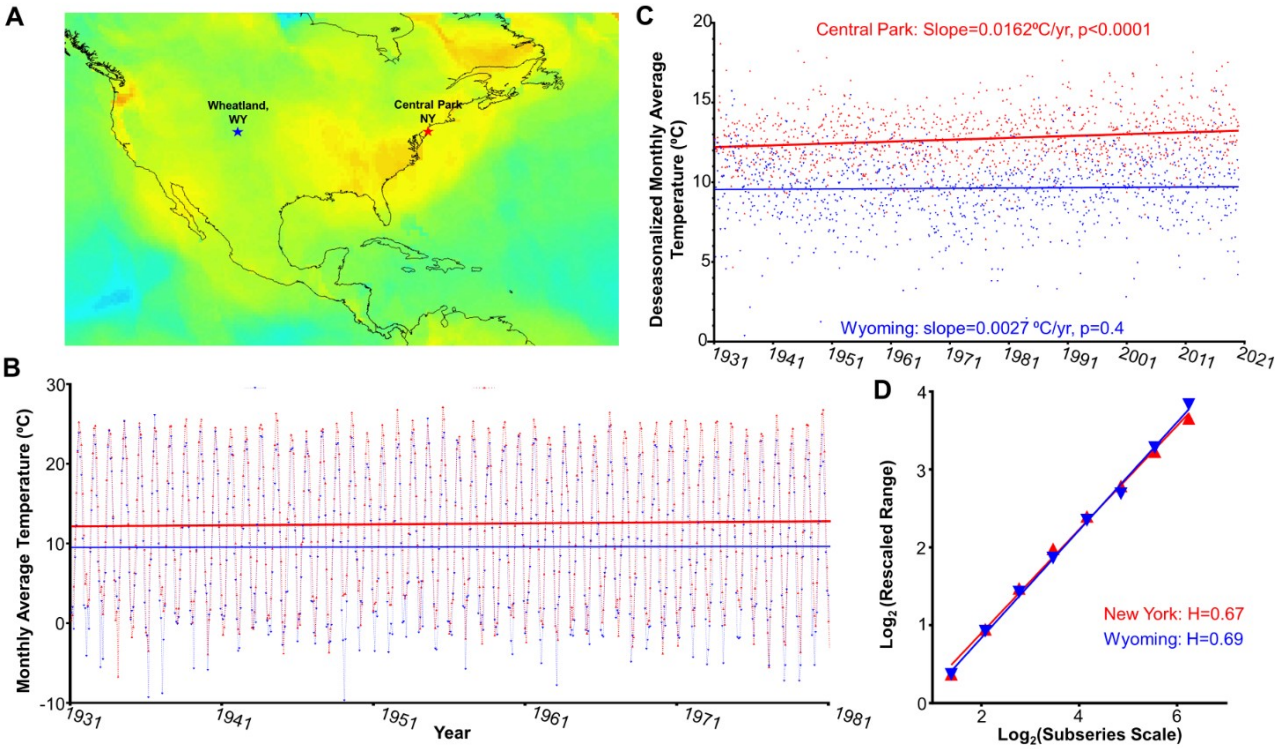

Fig. 3 Spatial Variations of Warming in the US. **A** Satellite imagery (October-November 2014) shows higher atmospheric CO_2 on the East and West Coasts than the Midwest. **B** Seasonal temperature cycles at Central Park, Manhattan (red) and Wheatland, Wyoming (blue). Central Park shows a higher and upward-shifting midline. **C** Post-deseasonalization, Central Park exhibits a faster warming rate (0.016 °C/year) compared to Wheatland (0.002 °C/year). **D** Rescaled range analysis reveals similar Hurst exponents for both locations.

mains [15]. However, Hurst exponent analysis is more tailored to detect long-term trends with computational simplicity. More importantly, it can provide a direct metric (Hurst exponent) for a more intuitive cross-regional comparison. This makes it fit the purpose of assessing heterogeneity better. Nevertheless, future research using STL or wavelet analysis is of great interest to elucidate the intricate interplay between ENSO and global warming.

The results of this study align with most current literature. According to the Sixth Annual Report (AR6) published by IPCC in 2023, the current average global warming rate is 0.02°C/year [1]. By applying a fractal approach, this study uncovered a wide range of warming rates (0.002 to 0.033°C/year). The Arctic is warming 16 times faster than Antarctica (0.033° vs. 0.002°/year). Unlike ice-covered Antarctica, the Arctic is an ocean with melting sea ice and significantly affects global sea levels. A novelty of our study is the use of the Hurst exponent to quantitatively gauge the strength of the warming trend in different regions. These results showed the Hurst exponents ranged from 0.66 to 0.82, suggesting a moderate to strong warming trend strength across the world. These findings challenge the so-called "Global warming hiatus", which claims that the current global warming is only temporary.

The temporal dynamics of global warming were also studied. Because the monthly average temperature records in Europe can be traced back to as early as the 18th century, they provide valuable information on how global warming evolved. A notable finding of this study was a 0.98°C temperature decrease in Milan, Italy from 1763 to 1862 ($p < 0.0001$) with a Hurst exponent of 0.72. This finding is consistent with the Little Ice Age theory [16]. However, post-Industrial Revolution, Milan warmed by 2.6°C from 1923 to the present ($p < 0.001$, $H = 0.82$). This reinforces the current view that contemporary global warming is most likely related to human population expansion and industrialization rather than the intrinsic natural temperature cycle of the Earth.

An additional interesting observation is that the 5.6% drop in global CO_2 emissions during the 2019 COVID-19 lockdowns had a minimal effect on the rising atmospheric CO_2 levels and global warming [10,17,18]. Because of its long atmospheric lifetime which spans from hundreds to thousands of years, CO_2 can accumulate and exert a prolonged influence on atmospheric

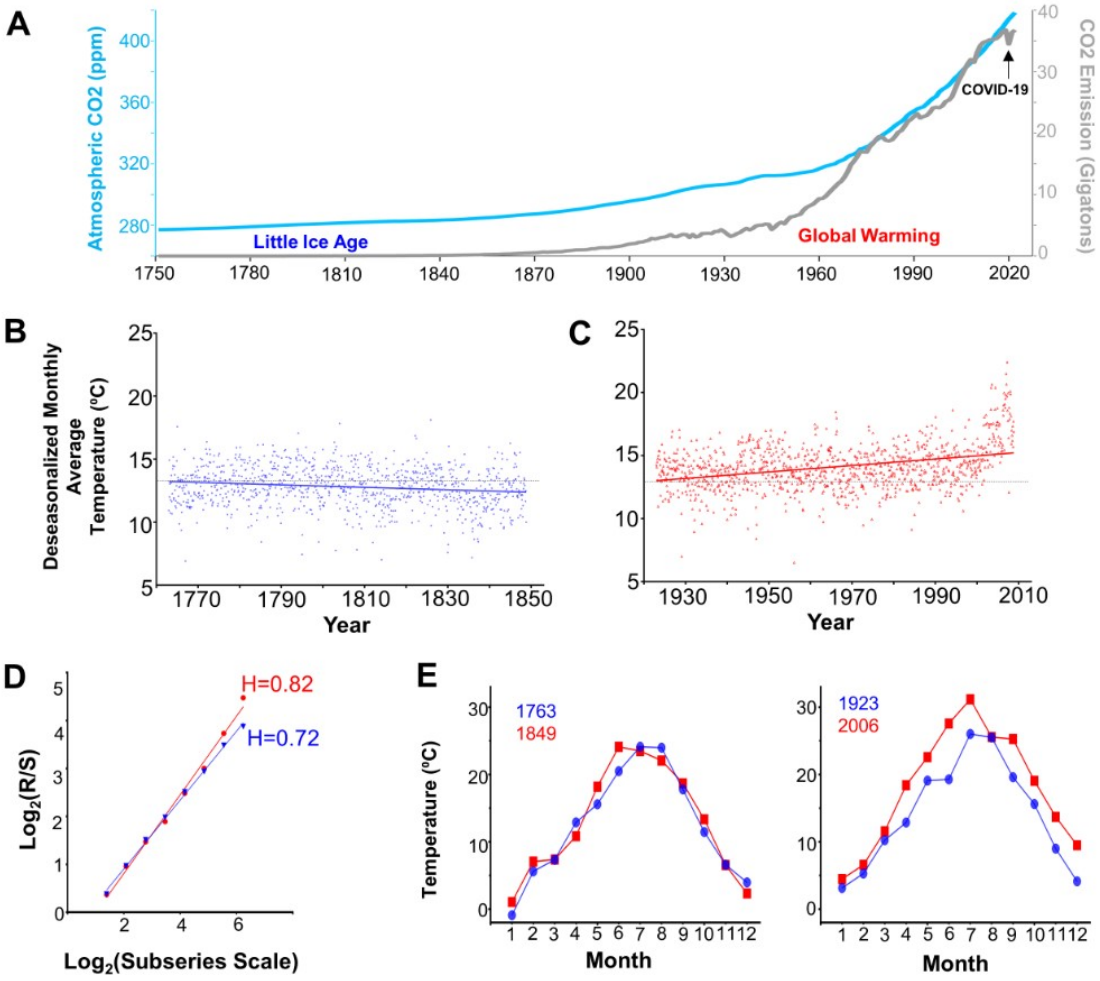

Fig. 4 Chronological Changes in Global Warming Dynamics. **A** The increase in global atmospheric CO_2 emission (gray line) and the corresponding increase of atmospheric CO_2 concentration (blue line) from 1750 to the current time. The 2019 pandemic lockdown resulted in a 5.6% reduction in emissions (indicated by an arrow), which did not significantly alter the upward trajectory of atmospheric CO_2 concentration levels. **B** Before industrialization, there was a cooling trend (0.01°C/year cooling) in Milan. **C** After industrialization, it became a warming trend (0.026°C/year warming) in Milan. **D** The temperature increase is more noticeable from April to September each year. In the pre-industrialization era, the monthly average temperatures in Milan showed no significant increase in each month each year. After industrialization, the most pronounced temperature increases were observed from April to September each year. **D** Rescaled range analysis for temperature change in the pre-industrialization (blue) and post-industrialization era (red). The Hurst exponents were 0.72 for the cooling trend in the pre-industrialization era and 0.82 for the warming trend in the post-industrialization era.

temperature. Therefore, a temporary dip in CO_2 emissions is unlikely to have a significant impact. This finding suggests that simply reducing emissions might not be sufficient to curb the current trajectory of global warming in the near term. More effective and sustainable decarbonization strategies are needed to achieve the Paris Agreement's goal of limiting the temperature rise within 1.5°C above the pre-industrial levels. Furthermore, while CO_2 is the primary GHG and accounts for ∼60% of global warming, it has a relatively modest GWP (global warming potential) value, estimated to be 1 over a century. In contrast, methane, the second leading GHG which accounts for ∼20% of global warming, is >80 times more potent than CO_2 over a 20-year span and >25 times more potent over a century[19]. Because of its much shorter atmospheric lifetime (∼ 10 years), methane can have a more immediate effect[20]. Interestingly, the 2020 global lockdown coincided with an unexpected surge in atmospheric methane levels, possibly due to increased emission from wetlands and decreased nitrogen oxide emission[21,22]. This

surge could amplify the global warming trend even with reduced CO_2 emissions in 2020. Therefore, it is critically important to address all GHGs holistically to combat global warming effectively.

The regional and temporal disparities of global warming and its impact bear important social and political implications. Since the Intergovernmental Panel on Climate Change (IPCC) was established in 1988, global efforts to combat climate change have focused on the "global commons" approach. While this has united countries in the fight, it fails to consider the uneven impact in different regions, making it hard to reach a consensus. The 2009 Copenhagen climate Summit's inability to set a shared greenhouse gas reduction goal illustrates this issue. Recently, some scientists have suggested shifting from the "global commons" to a "global fractal" approach[23]. This new paradigm acknowledges the multi-faceted nature of global warming and led to the more decentralized strategy of the 2015 Paris Agreement. The Agreement moves away from equal collective action and encourages countries to set unique goals suited to their specific circumstances.

This study also underscores the importance of climate inequality and provides some actionable insights. For example, the significantly faster warming rate in the Arctic calls for an urgent redirection of funds and resources to protect the communities there and intensify research into this Arctic amplification phenomenon. The six-time faster warming rate in NYC highlights the need for increased investment in public transportation and solar panels to mitigate GHG emission and urban heat island effect. Conversely, policies in the Midwest should be more tailored towards agricultural adaptation to increase the resilience to changing weather patterns. More importantly, areas with socioeconomic challenges may be significantly more vulnerable to the adverse impacts[24]. Because climate change is intricately linked with other major global challenges of our era, including inequality, environmental degradation, and security issues[25], it is crucial that policies and strategies are developed in a more holistic approach with a strong emphasis on inclusivity and justice for all communities[26].

Conclusion

In conclusion, by doing a comparative fractal analysis of deseasonalized monthly average temperatures worldwide, this study has illustrated significant variation in the impact of global warming across different regions and time periods. While global warming affects the entire planet, its effects are unevenly distributed, with some regions bearing a disproportionate burden. This underscores the critical need to address climate inequality and implement equitable, inclusive strategies to combat global warming. Shifting the perspective from viewing global warming as a straightforward problem to understanding it as the multifaceted, "global fractal" issue is crucial for taking a step in the right direction. This approach aligns with the Paris Agreement's decentralized strategy and emphasizes the importance of detailed research into the diverse aspects of climate change.

References

1 I.P.C.C., *IPCC*.

2 *Global Temperature Exceeds 20C Above Pre-Industrial Average on 17 November*.

3 M. Lynas, B. Houlton and S. Perry, *Environmental Research Letters*, **16**, 114005.

4 E. Foote, *American Journal of Science*.

5 R. Kaufman, M. Mann and S. Gopal, *PNAS*, **114**, 67–71.

6 Y. Guan, H. Lu, Y. Jiang, P. Tian, L. Qiu, P. Pellikka and J. Heiskane, *Ecological Indicators*, **130**, 108075.

7 B. Mandelbrot, *The Fractal Geometry of Nature*.

8 H. Hurst, *Transactions of American Society of Civil Engineers*, **116**, 770.

9 S. Gupta, N. Mastrantonas, C. Masoller and J. Kurths, *Chaos*, **32**, 052102.

10 *United Nations Environment Programme. COVID-19 caused only a temporary reduction in carbon emissions*.

11 C. Funk and B. Kennedy, *The Politics of Climate*, Pew Research Center.

12 L. Bodri, *Theor. Appl. Climatol*, **49**, 53–57.

13 W. Cai, A. Santoso, M. Collins, B. Dewitte, C. Karamperidou, J. Kug, M. Lengaigne, M. McPhaden, M. Stuecker, A. Taschetto, A. Timmermann, L. Wu, S. Yeh, G. Wang, B. Ng, F. Jia, Y. Yang, J. Ying, X. Zheng, T. Bayr, J. Brown, A. Capotondi, K. Cobb, B. Gan, T. Geng, Y. Ham, F. Jin, H. Jo, X. Li, X. Lin, S. McGregor, J. Park, K. Stein, K. Yang, L. Zhang and W. Zhong, *Nature Reviews Earth and Environment*, **2**, 628–644.

14 K. Cobb, C. Charles, H. Cheng and R. Edwards, *Nature*, **424**, 271–276.

15 Z. Morimoto and Z. Huang, *Hydrological Research Letters*, **2**, 70–74.

16 J. Mattews and K. Briffa, *Geografiska Annaler Series A Physical Geography*, **87**, 17–36.

17 C. Quéré, R. Jackson, M. Jones, A. Smith, S. Abernethy, R. Andrew, A. DeGol, D. Willis, Y. Shan, J. Canadell, P. Friedlingstein, F. Creutzig and G. Peters, *Nature Climate Change*, **10**, 647–653.

18 Z. Liu, Z. Deng., B. Zhu, P. Ciais, S. Davis, J. Tan, R. Andrew, O. Boucher, S. Arous, J. Canadell, X. Dou, P. Friedlingstein, P. Gentine, R. Guo, C. Hong, R. Jackson, D. Kammen, P. Ke, C. Quéré, C. Monica, G. Janssens-Maenhout, G. Peters, K. Tanaka, Y. Wang and H. Schellnhuber, *Nature Geoscience*, **15**, 615–620.

19 K. Mar, C. Unger, L. Walderdorff and T. Butler, *Environmental Science and Policy*, **134**, 127–136.

20 Z. Staniaszek, P. Griffiths, G. Folberth, F. O'Connor, N. Abraham and A. Archibald, *npj Climate and Atmospheric Science*, **21**, year.

21 S. Peng, X. Lin, R. Thompson, Y. Xi, G. Liu, D. Hauglustaine, X. Lan, B. Poulter, M. Ramonet, M. Saunois, Y. Yin, Z. Zhang, B. Zheng and P. Ciais, *Nature*, **612**, 477–482.

22 D. Stevenson, R. Derwent., O. Wild and W. Collins, *Atmospheric Chemistry and Physics*, **22**, 14243–14252.

23 S. Bernstein and M. Hoffmann, *Nature's Climate Change*, **9**, 919–925.

24 Y. Nunez, J. Benavides, J. Shearston, E. Krieger, M. Daouda, L. Henneman, E. McDuffie, J. Goldsmith, J. Casey and M. Kioumourtzoglou, *Nature Communications*, **15**, 268.

25 C. Kukowski and E. Garnett, *Nature Climate Change*, **14**, 2–4.

26 C. Zimm, K. Mintz-Woo, E. Brutschin, S. Hanger-Kopp, R. Hoffmann, J. Kikstra, M. Kuhn, J. Min, R. Muttarak, S. Pachauri, O. Patange, K. Riahi and T. Shinko, *Nature's Climate Change*, **14**, 22–30.